Macromolecular Architecture Effects on Block Copolymer Dynamics: Linear Tetrablocks and Inverse Starblocks

K. Chrissopoulou,[†,#] Y. Tselikas,[‡] S. H. Anastasiadis,[†,$] G. Fytas,[*,†] A. N. Semenov,[†,+] G. Fleischer,[§] N. Hadjichristidis,[†,‡] and E. L. Thomas[⊥]

Foundation for Research and Technology−Hellas, Institute of Electronic Structure and Laser, P.O. Box 1527, Heraklion Crete, Greece; Department of Chemistry, University of Athens, 157 01 Zografou Athens, Greece; Fakultät für Physik und Geowissenschaften, Universität Leipzig, D-04103 Leipzig, Germany; and Department of Materials Science and Engineering, Massachusetts Institute of Technology, Cambridge, Massachusetts 02139

Received January 26, 1999; Revised Manuscript Received May 4, 1999

ABSTRACT: Photon correlation spectroscopy and pulsed-field-gradient NMR have been used to investigate the role of different macromolecular architecture on the dynamics of block copolymer solutions in the low wavevector (q) limit using linear tetrablock (TB) and inverse starblock (SB) copolymers composed of two jointed TB's ($N_{SB} = 2N_{TB}$). The three relaxation processes observed for diblocks are also evident in the present case: the cooperative diffusion, the internal copolymer chain relaxation (q^2-dependent intensity and q-independent rate), and the polydispersity diffusive mode, controlled by the self-diffusion (due to the finite composition polydispersity). The internal mode characteristics are identical for both systems at a given concentration, in agreement with theoretical estimates for Rouse chains, whereas the self-diffusivities show the effect of the total molecular weight and the architecture. At high concentrations of the SB copolymers, there is evidence for an extra relaxation process with a strong-concentration-dependent intensity apparently due to the proximity to the ODT and due to the macromolecular architecture.

I. Introduction

Block copolymers represent an interesting class of polymeric materials with a rich variety of phase behavior[1] that is a consequence of the thermodynamic incompatibility between the covalently bonded linear sequences of polymerized monomers A and B. This leads to a disorder-to-order transition[2] (ODT) from a disordered state (at low enough values of χN) toward a microphase-separated state characterized by long-range order in its composition at higher χN values (N is the overall degree of polymerization and χ the segment−segment Flory−Huggins interaction parameter); the phase state depends on the volume fraction of the A block, f, as well.

The dynamic behavior of block copolymers has recently attracted a great deal of scientific interest,[3−6] with most of the work devoted to the study of diblocks. This can be addressed by probing either the spontaneous decay of composition fluctuations defining the dynamic structure factor $S(q,t)$ or the response of the system to external fields. At equilibrium, $S(q,t)$ of disordered diblock copolymer melts conforms[7] to a double-exponential decay function

$$S(q,t) = S_{int}(q) \exp(-\Gamma(q)t) + S_p(q) \exp(-Dq^2t) \quad (1)$$

with q the wavevector. The first exponential decay is the dynamic random phase approximation (RPA) prediction (for either Rouse[8] or entangled[9,10] chains) for monodisperse diblocks with $S_{int}(0) = 0$ and collective decay rate $\Gamma(q) \approx \tau_1^{-1}q^0$ for $q \ll q^*$, where q^* is the wavevector at the maximum of the static structure factor (τ_1 is the chain longest relaxation time). The second exponential is a consequence of the finite composition polydispersity of synthetic diblocks which, however, allows the determination of the chain self-diffusion coefficient $D \cong D_s$.

Solutions have long been used to complement the investigations of the diversity of phase morphologies and phase transitions[11−13] in diblock copolymers as well as of the dynamic structure factor,[14−17] where for neutral good solvents the unfavorable interactions between the blocks are diluted by the solvent, and therefore, the disordered state may be investigated even for high molecular weights at accessible temperatures ($\chi = a + b/T$ with $b > 0$). In semidilute solutions, χN is renormalized[13] as $\chi^* N \propto \chi N \phi^{(1-z)/(3\nu-1)} \cong \chi N \phi^{1.59}$, with ϕ the copolymer volume fraction in solution, ν the Flory exponent ($\nu = 0.59$ in good solvents), and $z = -0.225$; surprisingly, this renormalization was found to hold even for concentrations ϕ well into the concentrated solution regime.[11e] The bimodal shape of the dynamic structure factor of composition fluctuations $S(q,t)$ in eq 1 is still preserved whereas the total polymer concentration fluctuations relax via the cooperative diffusion $D_c \propto \phi^{\nu/(3\nu-1)} \cong \phi^{0.77}$, similarly to homopolymer semidilute solutions. For sufficiently high molecular weights, the dynamic structure factor of a monodisperse entangled diblock (the first exponential of eq 1) encompasses two distinct decays[10] corresponding to the chain slow repta-

* To whom correspondence should be addressed.
† Foundation for Research and Technology−Hellas.
‡ University of Athens.
§ Universität Leipzig.
⊥ Massachusetts Institute of Technology.
Also at Physics Department, University of Patras, 265 00 Rio Patras, Greece.
$ Also at Physics Department, University of Crete, 710 03 Heraklion Crete, Greece.
+ Permanent address: University of Leeds, Department of Applied Mathematics, Leeds LS2 9 JT, U.K., and Nesmeyanov Institute of Organo-Element Compounds of Russian Academy of Science, 28 Vavilova Str., Moscow 117812, Russia.

10.1021/ma9901083 CCC: $18.00
Published on Web 06/23/1999

tive motion (tube conformation) and to fast curvilinear displacements along the reptation tube (tube length fluctuations).

The effects of the macromolecular architecture on the static behavior of block copolymers have been considered[18,19] in the recent years, where going from diblocks to graft, triblock, and star copolymers increases their compatibility (i.e., increases the effective χN at the transition). Moreover, the macromolecular architecture (graft versus linear block copolymers) has been shown to alter the dependence of the microphase diagram on the volume fraction f.[20] At the same time, the morphological investigation of compositionally symmetric ($f \cong 0.5$) linear A−B−A−B tetrablock (TB) and inverse starblock copolymers (SB) essentially composed of two tetrablocks TB jointed in the middle point has revealed a triggering of the microstructure morphology by block asymmetry.[21] Macromolecular topology (e.g., stars) can also compensate the effect of molecular weight N on the molecular size and, hence, on the dynamics. The composition- and architecture-dependent self-diffusion coefficients of both graft and diblock copolymers in solution collapse nicely onto a master curve when the differences in the entanglement characteristics of the parent homopolymers and the different radii of gyration of stars versus linear polymers are taken into account.[22] Besides, keeping the block composition constant, macromolecular architecture affects the entropy of the chains and, thus, the static structure factor and the collective dynamics, whereas the more extended homogeneous range of star versus linear block copolymers may offer new insights in the dynamic behavior near the disorder-to-order transition.

In this report, we attempt to explore the effects of macromolecular architecture on the modes of relaxation of composition fluctuations in block copolymer solutions in a common good solvent by photon correlation spectroscopy (PCS) and pulsed-field-gradient nuclear magnetic resonance (PFG-NMR) utilizing the same linear A−B−A−B tetrablock and inverse starblock copolymers of ref 21. PCS provides simultaneous access to the dynamics of $S(q,t)$ over a broad time range (10^{-7}−10^{3} s) and the associated static structure factors. Provided that the composition fluctuations due to polydispersity (self-diffusion) and to the order parameter fluctuations (collective chain relaxation) are separable, $S_{int}(q)$ of an ideally monodisperse system can be determined at low wavevectors ($q < q^*$). The three relaxation processes known for diblock copolymer solutions are observed in this case as well, i.e., the cooperative diffusion, the internal copolymer mode, and the polydispersity diffusive mode. It is found that both the intensity and the relaxation rate of the internal mode are insensitive to both architecture and total molecular weight ($N_{SB} = 2N_{TB}$); this is theoretically explained to be due to the fact that linking together two tetrablocks into a single star does not change the "polarization" properties of each tetrablock chain. The self-diffusivities show the effect of the total molecular weight but not any extra exponential slowing down expected for stars because the present systems only reach the weakly entangled regime. Moreover, at high concentrations (still in the disordered state) and only for the inverse starblock copolymers, there is evidence for an extra relaxation process with a strong concentration dependence, apparently due to the proximity to the ODT and due to the macromolecular architecture.

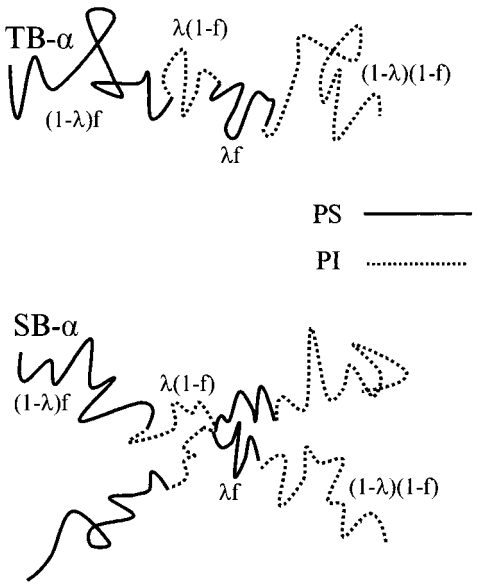

Figure 1. Schematic diagram of the linear tetrablock (TB) and the inverse (SB) starblock copolymers. The two shadings represent the polystyrene (PS) and the 1,4-polyisoprene (PI) sequences. Note that the SB is essentially composed of two TB molecules linked at the middle point. f is the volume fraction of polystyrene, and λ is the asymmetry parameter with the index $\alpha = (1 - \lambda)/\lambda$.

The remainder of this article is arranged as follows: Following the experimental section II, the results of the PCS and PFG-NMR investigations are presented in section III and are discussed in relation to a theoretical attempt to predict the behavior. The concluding remarks constitute section IV.

II. Experimental Section

Materials. The linear tetrablock and the inverse starblock copolymers, composed of styrene (PS) and isoprene (PI) sequences (Figure 1), were synthesized by anionic polymerization under high vacuum in glass reactors provided with break-seals (for the addition of reagents) and constrictions (for removal of products) utilizing the chlorosilane chemistry approach; their synthesis has been presented earlier.[21] The linear tetrablocks (TB) were synthesized by connecting a living $PIPS^{(-)}Li^{(+)}$ and a living $PSPI^{(-)}Li^{(+)}$ diblock arms to a dimethyldichlorosilane in solution in benzene, whereas the inverse starblocks (SB) were synthesized by connecting two living $PIPS^{(-)}Li^{(+)}$ and two living $PSPI^{(-)}Li^{(+)}$ diblock arms to a tetrachlorosilane. This approach has the advantage that the same diblock precursors were used for the synthesis of both the tetrablock and the inverse starblock, reensuring that the corresponding TB's and SB's have the same block components, and therefore, they are directly comparable. The resulting TB and SB were subsequently purified by fractionation in a toluene/methanol system.

The molecular weights of the polymers were determined by low-angle laser light scattering (LALLS) at 633 nm and membrane osmometry. The weight content of the polymers in PS was measured and verified by UV−SEC, ^{1}H NMR, and laser refractometry. The molecular characteristics of the linear tetrablocks and the corresponding inverse starblocks are presented in the three sections of Table 1. The first section concerns the molecular characteristics of the PSPI and the second the PIPS diblock precursors; the values in these two sections are the same for the linear tetrablock and the inverse starblock because the same precursors were used for their preparation. The results of molecular characterization show the high degree of structural and compositional homogeneity of these novel polymers. The macromolecular asymmetry is controlled by the parameter λ, which defines the volume

Table 1. Molecular Characteristics of the Copolymers[21]

samples	TB-1	SB-1	TB-2	SB-2	TB-4	SB-4
M_n(PS−PI) × 10^3 [a]	38.5	38.5	52.6	52.6	101	101
M_w/M_n(PS−PI)[b]	1.03	1.03	1.04	1.04	1.04	1.04
wt % PS content[c]	49.5	49.5	66.5	66.5	80.0	80.0
M_n(PI−PS) × 10^3 [a]	39.3	39.3	50.0	50.0	93.1	93.1
M_w/M_n(PI−PS)[b]	1.03	1.03	1.04	1.04	1.03	1.03
wt % PS content [c]	51.5	51.5	36.0	36.0	20.5	20.5
M_n(total) × 10^3 [a]	80.2	148	103	212	201	378
M_w(total) × 10^3 [d]	82.9	152	106	220	213	395
M_w/M_n(total)[b]	1.04	1.03	1.03	1.04	1.04	1.05
wt % PS content[c]	51.0	50.0	51.0	50.0	50.0	50.0
N_{tot}[e]	987	1812	1262	2623	2539	4709
f_{PS}[f]	0.475	0.465	0.475	0.465	0.465	0.470
λ	0.50	0.50	0.33	0.33	0.20	0.20
α	1	1	2	2	4	4
wt % ODT[g]	>46.4	55.6−62.6	>38.4	39.8−42.6	∼22.0	∼20.0

[a] Membrane osmometry in toluene at 34 °C. [b] SEC in THF at 30 °C. [c] UV−SEC and ^{1}H NMR. [d] LALLS in THF at 25 °C. [e] Based on average segmental volume. [f] Polystyrene volume fraction. [g] Estimated based on polarized and depolarized light scattering.[16,25]

fraction of the inner block of each diblock arm, with the volume fraction of the outer block being [1 − λ] (see Figure 1). The index (e.g., 4) in the codes for the tetrablock (TB) and the inverse starblock (SB) copolymers indicates the ratio $\alpha = (1 - \lambda)/\lambda$, i.e., the approximate ratio of the volume fractions of the outer to the inner block of the same kind (e.g., PS).

A relatively low concentration (∼2 wt %) copolymer solution in HPLC grade toluene solvent is initially prepared and filtered through a 0.22 μm Millipore filter directly into the dust-free light scattering cell (10 mm o.d.). During the measurements the cell was closed airtight to avoid evaporation of toluene. The concentration was checked before and after each measurement by weighing the solution. The concentration is then gradually increased by slow evaporation of small amounts of solvent and weighing the resulting solutions. All the measurements have been performed in the semidilute regime and in the disordered homogeneous state.

Photon Correlation Spectroscopy (PCS). The autocorrelation function of the polarized light scattering intensity, $G_{VV}(q,t) = \langle I_{VV}(q,t)\, I_{VV}(q,0)\rangle/\langle I_{VV}(q,0)\rangle^2$, with $I_{VV}(q,0)$ the mean light scattering intensity, is measured at different scattering angles, θ, using an ALV spectrophotometer and an ALV-5000 full digital correlator over the time range 10^{-7}−10^3 s. Both the incident beam from an Adlas diode pumped Nd:YAG laser, with wavelength λ = 532 nm and single mode intensity 100 mW, and the scattered beam were polarized perpendicular to the scattering plane (VV geometry). $q = (4\pi n_s/\lambda)\sin(\theta/2)$ is the magnitude of the scattering vector, with n_s the refractive index of the medium. In quasi-elastic light scattering under homodyne conditions, $G_{VV}(q,t)$ is related to the desired relaxation function, $C(q,t)$, by

$$C(q,t) = \{[G_{VV}(q,t) - 1]/f^*\}^{1/2} \tag{2}$$

where f^* is an experimental factor calculated by means of a standard. The amplitude (≤1) of the $C(q,t)$ is the fraction of $\langle I_{VV}(q,0)\rangle$ with decay times slower than about 10^{-7} s. For multiple relaxation processes, the experimental correlation functions may be analyzed by performing the inverse Laplace transform (ILT) of $C(q,t)$, without assumption of the shape of the distribution function $L(\ln \tau)$ but assuming a superposition of exponentials:

$$C(q,t) = \int_{-\infty}^{\infty} L(\ln \tau)\, \exp[-t/\tau]\, \mathrm{d}(\ln \tau) \tag{3}$$

This determines a continuous spectrum of relaxation times $L(\ln \tau)$; the average times obtained from the peaks of $L(\ln \tau)$ are used to determine the characteristic relaxation times, whereas the integrals under the peaks of $L(\ln \tau)$ give the dynamic intensities associated with the specific relaxation.

Pulsed-Field-Gradient Nuclear Magnetic Resonance (PFG-NMR). The basis of the technique is a stimulated echo measurement using the proton spin as a probe. PFG-NMR measures the mean-squared displacements $\langle \Delta r^2 \rangle$ of particles bearing ^{1}H nuclei in a given time t, if two magnetic field gradients are applied as pulses during the spin echo experiment.[23] The field gradients with amplitude $\mathbf{g}$ and width δ are separated by the diffusion time t (in the range 30−300 ms). If the motion of the particles is simple Fickian diffusion, then $\langle \Delta r^2 \rangle = 6D_s t$, and the translational self-diffusion coefficient D_s is obtained in the experiment. Deuterated toluene is used as the solvent for the copolymer solutions; thus, the diffusion of only the macromolecules is observed. From the measured spin echo attenuation, one can extract the Fourier transform of the autocorrelation function for the proton position which is identified with the normalized intermediate scattering function, $S_{inc}(q,t)$, usually measured by incoherent neutron scattering. Here, $\mathbf{q} = \gamma \mathbf{g} \delta$ is the generalized wavevector[24] with γ the gyromagnetic ratio of the proton (the range of q in the present experiments extends to about 1.0×10^{-3} Å^{-1}). $S_{inc}(q,t)$, was always to a very good approximation well represented by a single-exponential decay function (indicating a low molecular weight distribution), yielding the chain self-diffusion coefficient D_s

$$S_{inc}(q,t) = a_s \exp(-q^2 D_s t) \tag{4}$$

The $S_{inc}(q,t)$ data superimpose when plotted versus q^2t, and this signifies normal diffusion with mean-squared displacement $\langle \Delta r^2 \rangle \propto t$. Due to the presence of traces of protonated solvent molecules or residues of low molecular weight substances in the samples, a_s was in most cases slightly smaller but very near unity in the fits.

Dynamic Shear Rheology. A Rheometric Scientific ARES model 100FRTN1-HR controlled strain rheometer with a dual range force rebalance transducer was utilized in the parallel plates geometry (25 mm diameter, 0.7 mm sample thickness), with a recirculating fluids bath temperature control (accuracy ±0.5 °C). Measurements were carried out in a saturated atmosphere of the solvent (toluene) to prevent any adsorption of moisture and/or solvent evaporation from the sample. Small-amplitude oscillatory shear measurements were carried out in order to determine the linear viscoelastic properties of the solutions. More specifically, isothermal/isochronal dynamic time sweeps were performed to ensure that measurements were carried out under "dynamic equilibrium" conditions, dynamic strain sweeps at a given temperature and frequency in order to determine the limits of linear viscoelasticity (strains used were in the range 1−100%), and, finally, isothermal dynamic frequency sweeps in the frequency range 0.1−400 rad/s at a given strain in the linear viscoelastic regime in order to evaluate the dynamic mechanical material functions over the whole accessible frequency range.

III. Results and Discussion

Overall Picture. Figure 2 shows the net polarized intensity autocorrelation functions for a 9.5 wt % TB-

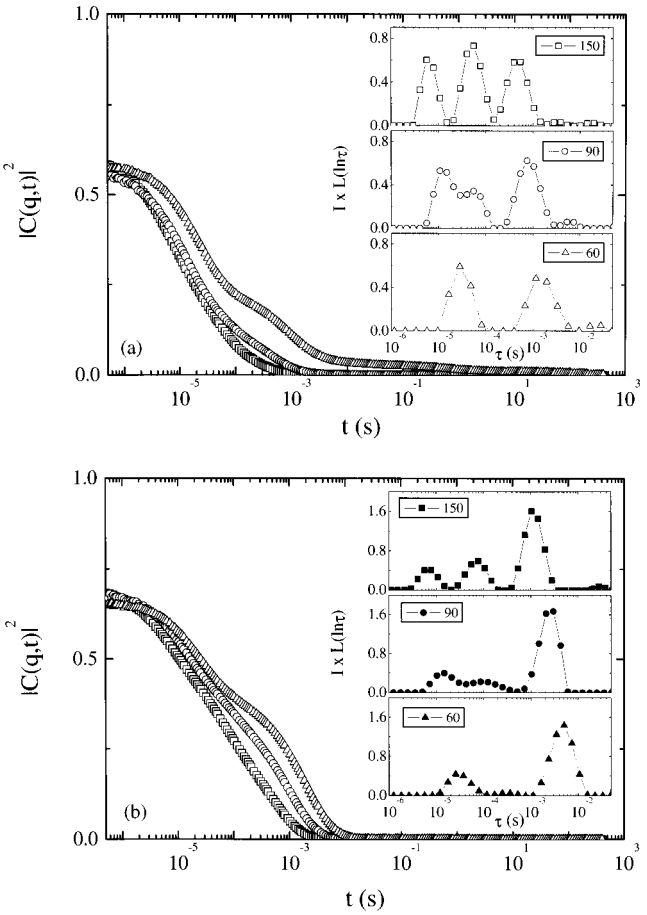

Figure 2. Net polarized intensity correlation functions for (a) a 9.5 wt % disordered TB-4/toluene solution and (b) a 9.5 wt % disordered SB-4/toluene solution at 20 °C for three different scattering angles: 150° (□, ■), 90° (○, ●), and 60° (△, ▲). Inset: the corresponding distributions of the relaxation times $L(\ln \tau)$ multiplied by the total scattering intensity normalized to that of toluene, I.

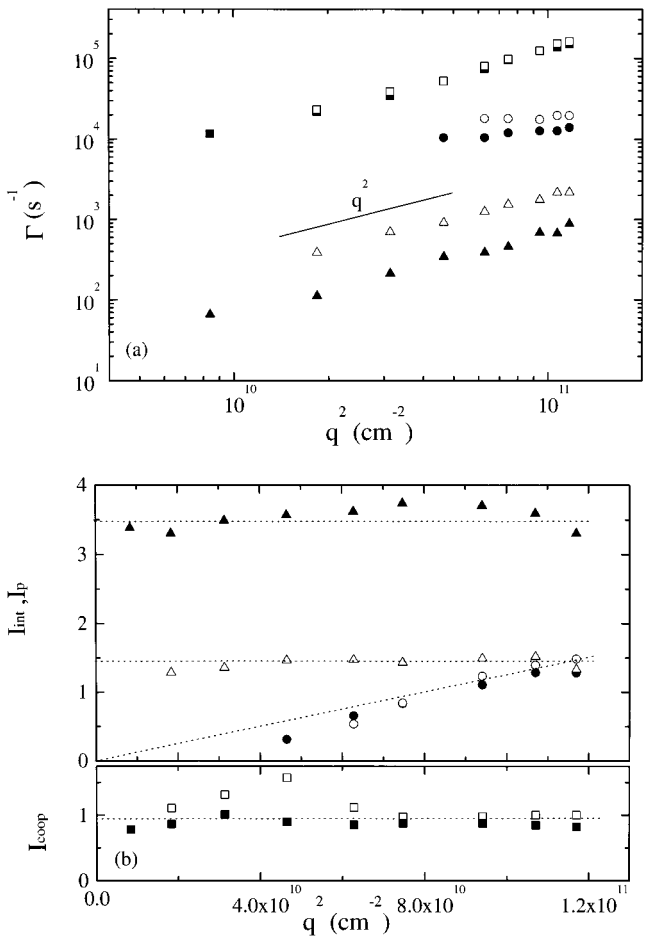

Figure 3. Wavevector dependence of (a) the relaxation rates and (b) the intensities of the three different processes (normalized to that of toluene) for the 9.5 wt % disordered TB-4/toluene (open symbols) and SB-4/toluene (closed symbols) solutions at 20 °C: (□, ■) cooperative diffusion, (○, ●) internal copolymer mode, and (△, ▲) polydispersity diffusive mode. The line in (a) shows the q^2 slope, whereas the dotted lines in (b) show the $I_{coop} \propto q^0$, $I_{int} \propto q^2$, and $I_p \propto q^0$ dependencies.

4/toluene (Figure 2a) and a 9.5 wt % SB-4/toluene solution (Figure 2b) for three different scattering angles with the corresponding distribution of relaxation times $L(\ln \tau)$ (eq 3) multiplied by the total polarized intensity normalized to that of toluene, I, shown in the insets; $I \times L(\ln \tau)$ facilitates comparison between the different scattering angles. In this range of concentrations the solutions exist in the disordered state as verified by the absence of dynamic depolarized light scattering.[25]

Three different relaxation processes are unambiguously resolved in both cases as well as for the other pairs similarly to diblock copolymer solutions. On the basis of the dependencies of the relaxation rates and the intensities of the three processes on the scattering wavevector (shown for both TB-4 and SB-4 solutions in Figure 3, a and b, respectively) and on concentration, these processes are assigned to the cooperative diffusion, the copolymer chain relaxation (internal), and the polydispersity mode (self-diffusion). The faster relaxation process exhibits a q^2-dependent relaxation rate and a q-independent intensity (Figure 3) and is attributed to the cooperative motion of the polymer network with respect to the solvent; this cooperative diffusion becomes faster with concentration while losing intensity since it is driven by the osmotic modulus of the polymer solution. It is the main mechanism to relax the total polymer concentration fluctuations and bears no specificity to block copolymer architecture; it will be of no further concern in the present paper. The two other processes are related to the dynamics of composition fluctuations (A versus B) and can be amenable to variation of the block copolymer architecture (see below). The intermediate process is the internal (structural) mode with a q^2-dependent amplitude and a q-independent relaxation rate at $q/q^* \ll 1$. The slower process shows a similar q dependence with the cooperative mode (q^2-dependent relaxation rate and q-independent intensity) and corresponds to the composition polydispersity mode observed in diblock copolymers in melt and in solution. This mode is responsible for the excess light scattering at low wavevectors whereas its diffusion coefficient compares well with the self-diffusivity of the block copolymer chains. In contrast to the cooperative diffusion, both the structural and the polydispersity modes become more evident as the concentration is increased. Differences and similarities in the composition fluctuation dynamics between the SB and TB copolymers will be discussed in the following.

Internal Structural Mode. The wavevector dependencies of the relaxation rates and the intensities of the internal and the self-diffusion processes for the TB-4 and SB-4 disordered solutions at similar concentrations (9.5 wt %) were shown in Figure 3. As stated above, the observed variation with the probing wavelength ($\sim q^{-1}$)

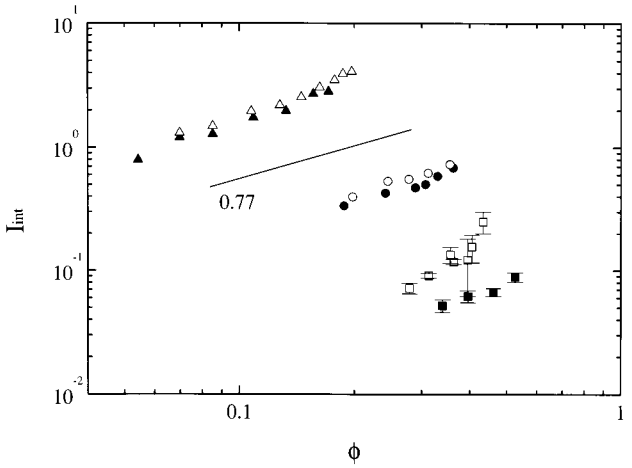

Figure 4. Copolymer concentration dependence of the intensity of the internal structural mode at 20 °C and 150° scattering angle for solutions in toluene of TB-4 (△), SB-4 (▲), TB-2 (○), SB-2 (●), TB-1 (□), and SB-1 (■). The solid line shows the predicted $\phi^{0.77}$ dependence. When error bars are not shown, they are less than or equal to the size of the points.

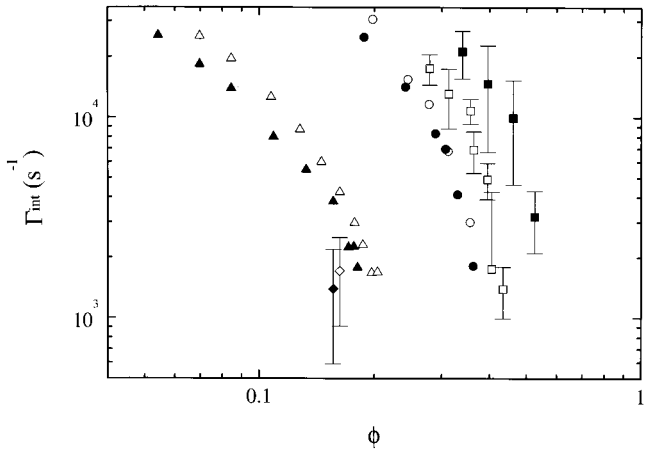

Figure 5. Copolymer concentration dependence of the relaxation rate of the internal structural mode at 20 °C and 150° scattering angle for solutions in toluene of TB-4 (△), SB-4 (▲), TB-2 (○), SB-2 (●), TB-1 (□), and SB-1 (■). The inverse of the longest relaxation times estimated by dynamic oscillatory shear rheology for one concentration of TB-4 (◇) and SB-4 (◆) are also included. When error bars are not shown, they are less than or equal to the size of the points.

is characteristic for these two processes observed for diblock copolymers in semidilute solutions in a common good solvent. The correct separation of the two contributions to the experimental $S(q,t)$ leads to the anticipated correlation hole in the limit of $q \rightarrow 0$ for monodisperse block copolymers; note that the total static intensity measurements (inclusion of all kinds of contributions) lead to finite $I(q\rightarrow 0)$. The intensity I_{int} of the structural relaxation exhibits a q^2 dependence imposed by the A−B connectivity. Concurrently, the average collective relaxation rate[8,10] estimated within the RPA (for Rouse diblock chains in the melt) is given by

$$\Gamma_{int}(q) = q^2 \frac{k_B T}{N\bar{\xi}} \frac{f(1-f)g(1,x)}{I_{int}(q)/N} \qquad (5a)$$

where $k_B T/\bar{\xi}$ is the monomeric diffusion coefficient (for Rouse chains, $k_B T/(N\bar{\xi})$ is the chain diffusivity D_s), $g(1,x)$ is the Debye function of the copolymer chain with $x = q^2 R_g^2$ and R_g the copolymer radius of gyration, and the $I_{int}(q)/N$ factor[26] denotes the collective (thermodynamic) effect. If one uses the longest relaxation time of a respective homopolymer $\tau_1 \approx R_g^2/(6D_s)$, eq 5a can also be written as

$$\Gamma_{int}(q) = \frac{xf(1-f)g(1,x)}{6\tau_1 I_{int}(q)/N} \qquad (5b)$$

In the $q/q^* \ll 1$ range, $g(1,x) \cong O(1)$ and $I_{int}(q)/N \propto x$, and therefore, $\Gamma_{int}(q) \approx \tau_1^{-1}[4f(1-f)]^{-1}q^0$ as verified by dynamic mechanical shear measurements (see Figure 5). What was unexpected is the apparent similarity of both the intensities and the relaxation rates of the intermediate internal mode despite the architecture and the total molecular weight difference between TB-4 and SB-4 (as well as for the other pairs—see Figures 4 and 5). Regarding the slower polydispersity mode, both the rates and the intensities are different in the two systems (see discussion below). The q dependencies shown in Figure 3 for TB-4 and SB-4 also apply to the other two SB and TB pairs.

Physically, the scattering due to the internal mode results from composition fluctuations caused by the relative motion or "breathing" of the A blocks with respect to the B blocks. The general equation for the intensity at low wavevectors,[10] $I_{int} \propto \phi N q^2 R_g^2$, can be written as

$$I_{int} \propto \frac{\phi}{N_{tot}\upsilon} q^2 \kappa \qquad (6)$$

where a prefactor related to the A−B contrast is omitted in eq 6. $[\phi/(N_{tot}\upsilon)]$ is the number of copolymer chains per unit volume where $N_{tot} = N$ for the tetrablock TB and $N_{tot} = 2N$ for the starblock SB is the total number of monomers per chain, and κ is the effective "polarizability" of the block copolymer chain, which can be defined as follows.

Let a weak force be applied to each monomer of a block copolymer chain. Then, the force acting on the nth monomer is $F(n) = \epsilon h(n)$, where ϵ is a small amplitude and $h(n) = 1 - f$ if the nth monomer is of type A and $h(n) = -f$ if it is of type B. Here $n = 0, 1, 2, ..., N_{tot}$ and f is the volume fraction of A monomers in a chain. Thus, each A monomer is subjected to the force $(1 - f)\epsilon$, and each monomer B to the force $-f\epsilon$, so that the total algebraic force acting on the chain is zero. The chain "polarization" is defined as $\mathbf{P} = \sum_n \mathbf{r}(n)h(n)$, where $\mathbf{r}(n)$ is the position of the nth monomer. The average polarization induced by the force $F(n)$ is proportional to ϵ, with the coefficient being κ: $P = \kappa\epsilon$. With the above definition, the effective "polarizability" κ can be directly calculated using Gaussian chain statistics as

$$\kappa_{TB} = {}^2/_3 a^2 N_{tot,TB}{}^3 f^2(1-f)^2[1 - 6\lambda^2(1-\lambda)] \qquad (7a)$$

$$\kappa_{SB} = {}^1/_4 \cdot {}^2/_3 a^2 N_{tot,SB}{}^3 f^2(1-f)^2[1 - 6\lambda^2(1-\lambda)] \qquad (7b)$$

for the tetrablock and the starblock, respectively. Here $a = \beta^*/\sqrt{6}$, and $\beta^* \approx b\phi^{-0.117}$ is the effective statistical segment length in solution with b that in the bulk, assumed to be equal for both components A and B. The macromolecular asymmetry affects the effective polarizabilities κ through the parameter λ.

Since in the present experimental system ($N_{tot,SB} = 2N_{tot,TB}$), eqs 7 result in

$$\kappa_{SB} = 2\kappa_{TB} \tag{8}$$

Therefore, with eq 6, one gets exactly the same intensity for the SB and the TB solutions at a fixed polymer concentration, and therefore

$$I_{int,SB} = I_{int,TB} = {}^2/_3\frac{\phi}{v}a^2q^2N^2f^2(1-f)^2[1-6\lambda^2(1-\lambda)] \tag{9}$$

Note that $a^2 = b^2\phi^{-0.234}/6$, and therefore, $I_{int} \propto \phi^{0.77}$. For $\lambda = 0$ or 1, the result is simplified to the appropriate expression for a diblock copolymer with N segments. Recently, a random phase approximation calculation[27] was performed for the full static structure factor for linear tetrablocks and inverse starblock copolymers as a function of both the block copolymer composition and the detailed architecture controlled by the parameter λ. (The case of two different ratios of the outer to the inner block for A and B was also considered.) The results for the behavior at low wavevectors are identical to those of eq 9, i.e., $I_{int,SB} = I_{int,TB}$, irrespective of the values of the two different ratios of the outer to the inner block. It should also be noted that connecting the two TB chains in order to form one SB chain leads to a lower entropy for SB, resulting in weaker composition fluctuations when compared to the case of TB; this is reflected in the fact that the static structure factor[26] $S(q) \propto I_{int}/(\phi N_{tot})$ of the starblocks at low wavevectors is according to eq 9 one-half of that for the tetrablocks. Moreover, the higher compatibility of the starblock is also evident by the fact that the predicted[27] value of the product $(\chi^* N_{tot})_s$ at the mean-field spinodal for the starblock is twice as large as that for the respective tetrablock for near-symmetric systems; in the present case $N_{tot,SB} = 2N_{tot,TB}$ and hence $\chi^*_{s,SB} = \chi^*_{s,TB}$.

The experimental data for the intensities of the internal mode at 150° scattering angle ($q = 0.034$ nm^{-1}) as a function of copolymer concentration are shown in Figure 4 for the three SB and TB pairs. The equality of the intensities of the modes between SB-4, TB-4 and SB-2, TB-2 is in agreement with the above theoretical estimation whereas the comparison for the lowest molecular weight system SB-1, TB-1 is less satisfactory. Note, however, the very low values of the intensities for SB-1, TB-1 with the corresponding significantly higher associated errors; moreover, the resolution of the internal mode in SB-1 is affected by the extra process discussed later. Besides, the intensities conform to the predicted $I_{int} \propto \phi^{0.77}$ dependence.

Figure 5 shows the q-independent relaxation rates of the internal process as a function of concentration for the three SB, TB pairs. The relaxation rates for the inverse starblocks are very similar to those for the tetrablocks over the whole concentration range although the former possess double the molecular weight of the latter. As was discussed above, the relaxation time of the internal mode for symmetric diblock copolymers is equal to the longest relaxation time which is a function of the molecular weight ($\tau_1 \propto N^2$ in the Rouse and $\tau_1 \propto N^3$ in the entanglement regime).

For the calculation of the average relaxation rates of the internal mode in TB and SB, Rouse dynamics is assumed; i.e., it is assumed that entanglement effects are not important in this range of concentrations.[22] The relaxation time for the internal mode is actually the time for relaxation of the "polarization" after the external force is switched off. For homogeneous TB and SB melts, this can be calculated within the dynamic random phase approximation similarly[8] to the case of diblock copolymers and polymer blends for Rouse chains. In the limit of low wavevectors, this calculation results in the average rate

$$\Gamma_{int,SB}(q) = \Gamma_{int,TB}(q) = \frac{k_BT}{N\bar{\xi}}\frac{3}{2f(1-f)(Nb^2/6)}[1-6\lambda^2(1-\lambda)]^{-1}q^0 \tag{10a}$$

i.e., as expected, the relaxation time does not depend on the wavevector and is identical for the SB and TB systems of the present work. (Equation 10a can also be obtained using eqs 9 and 5a in the low q limit with $g(1,x) \rightarrow 1$.) This rate is only by a factor $[1-6\lambda^2(1-\lambda)]^{-1}$ larger than that for the respective diblock of molecular weight equal to that of the tetrablock; this is the same factor that controls the effect of copolymer architecture on the intensity of either SB or TB (eq 9). For semidilute solutions in the Rouse regime, eq 10a is renormalized as

$$\Gamma_{int,SB}(q) = \Gamma_{int,TB}(q) = \frac{3D_{s,lin}}{2f(1-f)Na^2}[1-6\lambda^2(1-\lambda)]^{-1}q^0 \approx \frac{[1-6\lambda^2(1-\lambda)]^{-1}}{4f(1-f)\tau_{1,lin}}q^0 \tag{10b}$$

where $D_{s,lin}$ and $\tau_{1,lin}$ are the self-diffusivity and the longest relaxation time of a linear chain with molecular weight equal to that of the tetrablock. Physically the equality of the relaxation times for the tetrablock and the starblock can be understood as being due to the fact that the two tetrablocks that compose the starblock relax their polarization virtually independently; since the two tetrablocks are identical, they relax exactly in parallel, and the fact that they are linked in the middle does not make any difference. Experimentally (Figure 5), the relaxation rates of the internal mode in the SB-4 system are only somewhat slower (by about 30−40%) than in the TB-4 system, whereas the data for the other two pairs are in perfect agreement with the predictions of eq 10b. Note that the anticipated ratio between TB and SB based only on the molecular weight should be at least (Rouse regime) a factor of 4.

The agreement between the relaxation rates of composition fluctuations Γ_{int} for the SB and TB pairs ($N_{tot,SB} = 2N_{tot,TB}$ and the same f and λ) suggests that their longest relaxation times τ_1 should also assume similar values, since Γ_{int} is related to τ_1 (eq 5b). On the theoretical side, the longest time of conformational relaxation can be calculated within the Rouse model for the tetrablock and the starblock copolymers. In the limit of the same individual segmental frictions for the two blocks (this assumption is allowed, since we will then renormalize the situation for semidilute solutions), the situation leads to the calculation for the Rouse time of homopolymer stars with four arms. In the general case of a star with f_s equal arms,

$$\tau_{1,star} = \frac{4}{f_s^2}\tau_{1,linear} \tag{11}$$

in agreement with earlier estimates.[28] Here, $\tau_{1,linear}$ is the Rouse time of a linear chain with molecular weight

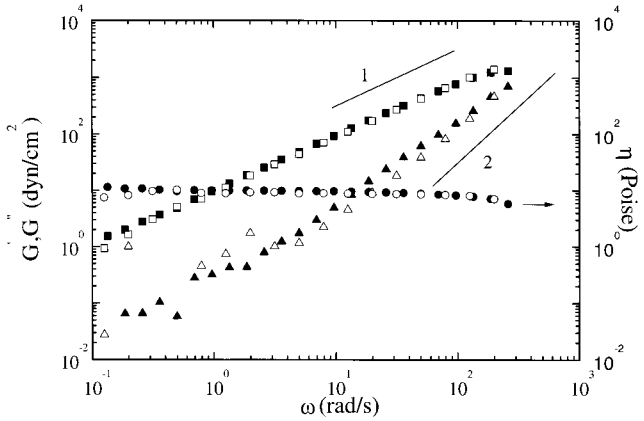

Figure 6. Dynamic frequency sweep for disordered 17.9 wt % TB-4/toluene (open symbols) and 17.27 wt % SB-4/toluene (closed symbols) solutions at 20 °C; the applied strains were 40% and 10% for SB-4 and TB-4, respectively: G' (△, ▲), G'' (□, ■), and $\eta = G''/\omega$ (○, ●). The lines show the $G' \sim \omega^2$ and $G'' \sim \omega$ behavior in the flow regime.

equal to that of the whole star. Therefore, for our system of SB and TB with $N_{tot,SB} = 2N_{tot,TB}$ and $f_s = 4$, it is expected that in the Rouse regime

$$\tau_{1,SB} = \tau_{1,TB} \tag{12}$$

The inverse of the longest relaxation times obtained by low-amplitude dynamic oscillatory shear rheology at one concentration for each of the TB-4/toluene and SB-4/toluene solutions are also shown in Figure 5; the times were estimated at the crossing of the dynamic shear storage (G') and loss (G'') moduli in the flow regime. Figure 6 shows a dynamic frequency sweep for disordered 17.9 wt % TB-4/toluene and 17.27 wt % SB-4/toluene solutions at 20 °C. At low frequencies the data in both cases conform to the expected $G' \sim \omega^2$ and $G'' \sim \omega$ scaling behavior for disordered systems. This allows the extrapolation of the G' and G'' data in order to estimate the longest relaxation time, which were shown in Figure 5. In agreement with eq 12, the two times are almost the same (within the experimental errors). The viscosity shown in Figure 6 was obtained from G'' as $\eta = G''/\omega$, and its independence of frequency for low frequencies is due to the systems having attained their limiting behavior. (The zero shear viscosity is, then, $\eta_0 = \lim_{\omega\to 0}[G''/\omega]$.) The viscosities of both systems are very similar. (The data for SB-4 are only slightly higher than for TB-4.) For Rouse chains the zero shear viscosity of a homopolymer star[28,29] $\eta^0_{star} = g\eta^0_{linear}$, where g is the ratio of the square of the radius of gyration of the star to that of the linear molecule with the same molecular weight. For a star with f_s equal arms, g is calculated as $g = (3f_s - 2)/f_s^2$, and for a four-arm star $g = 0.625$. Since for Rouse chains $\eta^0_{linear} \propto N_{tot}$, the ratio of the zero shear viscosities of SB and TB should be $\eta^0_{SB}/\eta^0_{TB} = 2g = 1.25$, in agreement with the closeness of the viscosity data in Figure 6.

The observed agreement between the two Γ_{int}'s (PCS) and the two τ_1's (rheology) and the obtained theoretical account suggest very minor entanglement effects. It is noted that in the really entangled regime the conformational relaxation of stars is exponentially suppressed;[30] however, in the present range of concentrations of 5−20%, the estimated number of entanglements per chain is only 1−3 (see also Figure 11), far from the range where entanglement effects become really important.

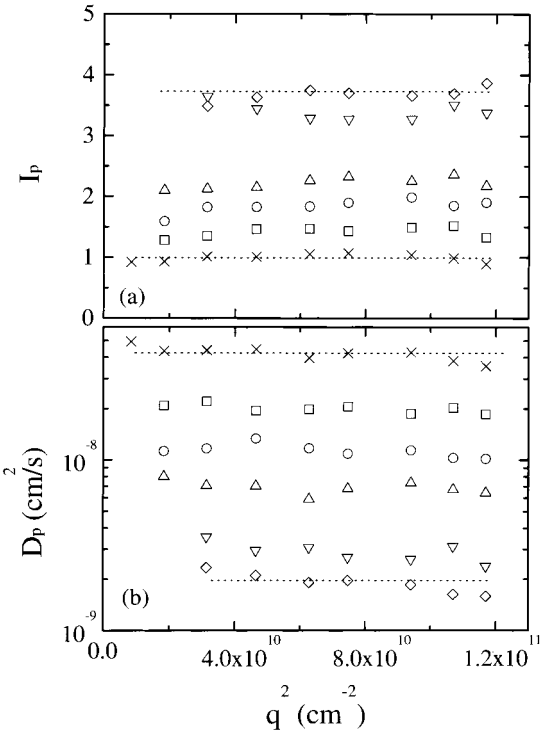

Figure 7. Wavevector dependence of (a) the intensities and (b) the diffusion coefficients of the polydispersity diffusive process for various concentrations of the TB-4/toluene solution at 20 °C: (×) 6.1, (□) 9.5, (○) 11.9, (△) 14.7, (▽) 17.9, and (◇) 19.6 wt %. Dotted lines are guides to the eye and denote q-independent intensities and diffusion coefficients.

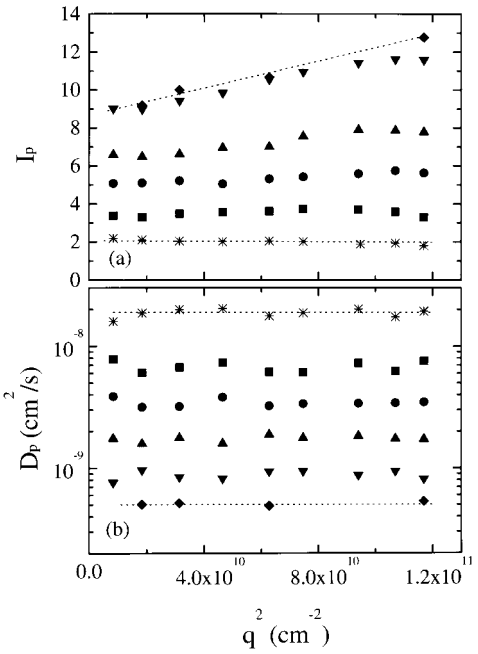

Figure 8. Wavevector dependence of (a) the intensities and (b) the diffusion coefficients of the polydispersity diffusive process for various concentrations of the SB-4/toluene solution at 20 °C: (*) 6.1, (■) 9.5, (●) 12.1, (▲) 14.7, (▼) 17.3, and (◆) 18.9 wt %. Dotted lines are guides to the eye (see text).

Polydispersity (Self-Diffusion) Mode. Figures 7 and 8 show the wavevector dependencies of the intensities and the corresponding diffusion coefficients for the polydispersity diffusive relaxation for the TB-4/toluene and SB-4/toluene solutions, respectively, as a function of total copolymer concentration. The behavior for the

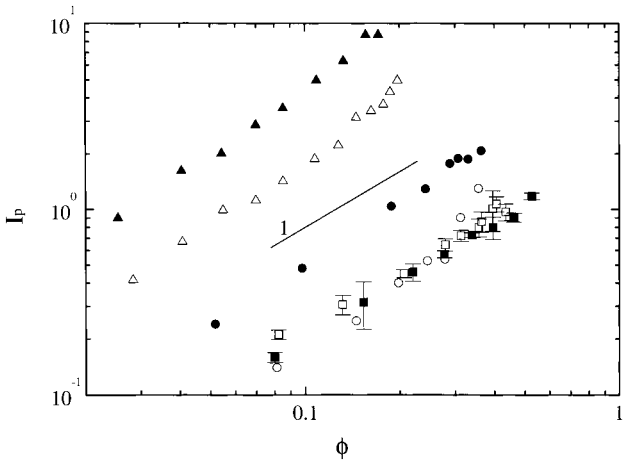

Figure 9. Copolymer concentration dependence of the intensity of the polydispersity diffusive mode at 20 °C for solutions in toluene of TB-4 (△), SB-4 (▲), TB-2 (○), SB-2 (●), TB-1 (□), and SB-1 (■). The solid line denotes the ϕ^1 dependence. When error bars are not shown, they are less than or equal to the size of the points.

TB-4/toluene system conforms exactly to the known behavior, i.e., q-independent intensities (Figure 7a) increasing with copolymer concentration and diffusion coefficients ($D_p = \Gamma_p/q^2$) decreasing with increasing concentration (Figure 7b). The same is true for the SB-4/toluene for concentrations as high as about 10 wt %. However, at higher concentrations, there is a pronounced peculiar increase of the intensity at higher wavevectors (Figure 8a), which is almost linear with q^2. Note that the possibility of an extra slow process similar to the frequently observed "long-range density fluctuations" would result in the opposite dependence with q. It appears that a q^2-dependent contribution (due to a possible unresolved process) is superimposed on a q-independent term (which would conform with the behavior of the polydispersity mode). Such a contribution to the scattering intensity, with behavior similar to that of the internal mode, should be of structural origin. Information on the possible origin of this extra contribution is also provided by the concentration dependence of its extra intensity (see next section). Note, however, that the dynamics of the process is not affected; i.e., the relaxation rates still show a $\Gamma_p \propto q^2$ dependence evident by the q independence of the diffusion coefficient D_p (Figure 8b).

The intensities of the polydispersity process for all three SB, TB pairs are shown in Figure 9 as a function of concentration. For the high concentrations of SB-4, where the intensities show a wavevector dependence, the values of the limits $I_p(q\rightarrow 0)$ are used in Figure 9 following a fit of the data to the form $I_p(q) = I_p(q\rightarrow 0) + Cq^2$. An almost linear dependence of the intensities on copolymer concentration is seen. The intensity of the polydispersity mode is independent of the wavevector and is proportional[7,31] to the total number of monomers per chain N_{tot} and to the effective degree of composition polydispersity, $\Delta = 4\langle(f - \bar{f})^2\rangle$, where $\bar{f}$ is the mean composition:

$$I_{p,TB} \cong \frac{\phi}{v} N_{tot}\Delta = \frac{\phi}{v} N\Delta \qquad (13)$$

for tetrablocks. For starblocks, one should substitute N by $2N$ and take into account a possible change in Δ. If one assumes that the composition fluctuations $\delta f = f - \bar{f}$ of the two tetrablocks that compose a starblock are statistically independent, one can get $\Delta_{SB} = \Delta_{TB}/2$, which would predict the same intensity for the polydispersity mode for TB and SB systems.

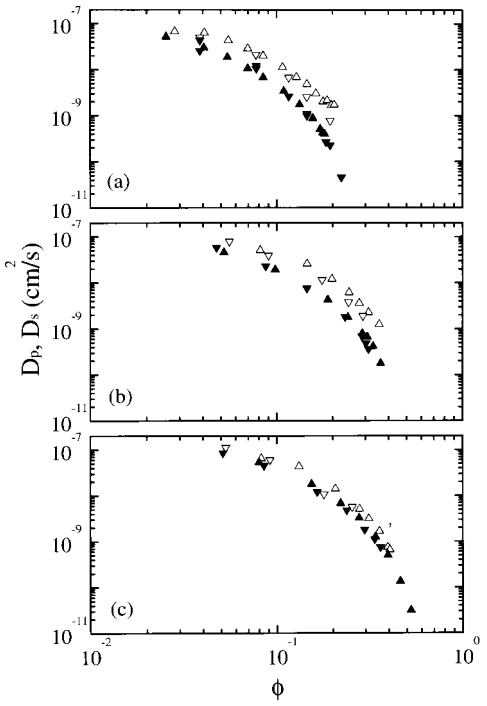

Figure 10. Copolymer concentration dependence of the diffusion coefficients of the polydispersity mode, D_p, and the copolymer self-diffusivity measured by PFG-NMR, D_s, at 20 °C for solutions in toluene of (a) TB-4 and SB-4, (b) TB-2 and SB-2, and (c) TB-1 and SB-1. In all three, (△) D_p of TB, (▲) D_p of SB, (▽) D_s of TB, and (▼) D_s of SB. The error bars are less than or equal to the size of the points.

Experimentally (Figure 9), the intensity of the polydispersity mode for the SB-4 solutions is about 2.5−3 times higher than that for the TB-4 with this difference becoming less for SB-2/TB-2 and almost nonexistent for the SB-1/TB-1 pair. A higher intensity for the SB system may be expected if the composition fluctuations in the two tetrablock parts of the starblock are correlated. The strongest correlation implies that $\Delta_{SB} = \Delta_{TB}$ and, thus, $I_{p,SB} = 2I_{p,TB}$; however, there is in principle no apparent reason for that strong correlation of composition fluctuations. The above treatment assumes that the composition polydispersity for the starblock originates only from the composition polydispersity of the linear tetrablock. However, due to the complicated synthesis procedure,[21] other sources of composition polydispersity may contribute as well. At any rate, I_p/N_{tot} vs ϕ (eq 13) is currently the most reliable measure of composition polydispersity (Δ) in block copolymers.

Figure 10 shows the concentration dependencies of the diffusion coefficients of the polydispersity mode, D_p, for the three SB/TB pairs together with the self-diffusion coefficients, D_s, measured by PFG-NMR. Note that the dynamics of the polydispersity mode (Figure 8b) is still diffusive even at the high concentrations of SB-4, even when the intensities of the mode show the peculiar behavior discussed above in relation to Figure 8a. In contrast to the data for the internal mode, the diffusion coefficients show the effect of the different molecular weights of the SB and TB systems. The self-diffusion coefficients show very similar behavior with the poly-

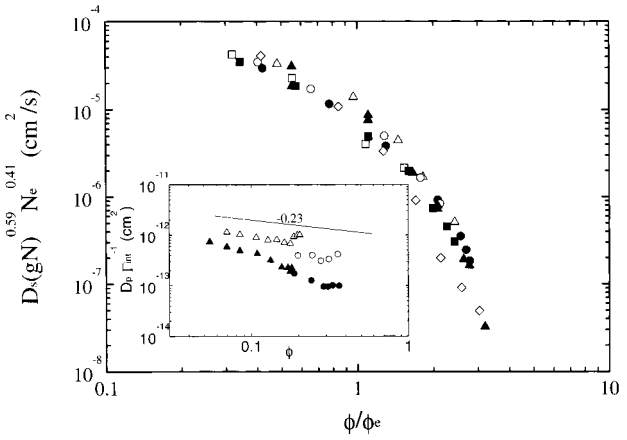

Figure 11. Self-diffusion coefficients of solutions in toluene of TB-4 (△), SB-4 (▲), TB-2 (○), SB-2 (●), TB-1 (□), and SB-1 (■) as well as of SI-57 diblock[22] (◇) in the representation $[D_s(gN)^{0.59}N_e^{0.41}]$ versus $[\phi/\phi_e]$ with $\phi_e = [N_e/(gN)]^{0.77}$. Inset: concentration dependence of the product $D_p\Gamma_{int}^{-1}$ for solutions in toluene of TB-4 (△), SB-4 (▲), TB-2 (○), and SB-2 (●) with the line denoting the expected $\phi^{-0.23}$ dependence. The error bars are less than or equal to the size of the points.

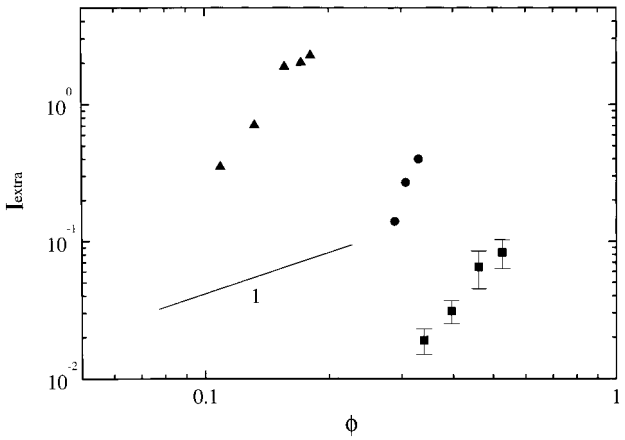

Figure 12. Concentration dependence of the intensity associated with the "extra process": for SB-4, the extra intensity contribution to the apparent intensity of the polydispersity mode $\{I_p(q) - I_p(q\rightarrow 0)\}$ is shown at 90° (▲) scattering angle. For SB-2 (●) and SB-1 (■), the angle-independent intensities of the new intermediate mode are shown. The solid line denotes the ϕ^1 dependence not followed by the data. When error bars are not shown, they are less than or equal to the size of the points.

dispersity diffusion coefficients, and the agreement between D_p and D_s for all samples is very good.

The relaxation of the "polydispersity" composition fluctuations proceeds via the self-diffusion of the copolymer chains,[16,31] with the predicted rate $\Gamma_p = D_p q^2 \cong D_s q^2$ for small Δ. Within Rouse dynamics the self-diffusion coefficient is just inversely proportional to the molecular weight, i.e., $D_s = D_0/N_{tot}$, where D_0 is the effective monomer mobility (renormalized by the presence of the solvent). Therefore, the prediction for the SB and TB pair is $D_{s,SB} = 0.5D_{s,TB}$. Experimentally, the ratios of the diffusivities of SB to TB vary from 0.7 (4 wt %) to 0.3 (20 wt %) for SB-4 and TB-4 and 0.7 (5 wt %) to 0.25 (30 wt %) for SB2 and TB-2; it is around 0.7 for SB-1 and TB-1. In principle, the smaller size of star molecules compared to linear ones of the same molecular weight should be taken into account together with the characteristic concentration for entanglements.[22] The effect of macromolecular architecture on the self-diffusion coefficients for copolymeric systems was indeed investigated before for diblock and simple graft copolymers.[22] There, it was suggested that for not-well-entangled solutions the different entanglement characteristics of the parent homopolymers as well as the smaller size of star molecules compared to linear ones should be taken into account. The self-diffusion data would collapse onto a master curve when plotted as $[D_s(gN)^{\nu}N_e^{1-\nu}]$ versus $[\phi/\phi_e]$ with ϕ_e the characteristic concentration for entanglements, $\phi_e = [N_e/(gN)]^{3\nu-1}$, where ν is the Flory exponent ($\nu = 0.59$ for good solvents), N_e is the number of segments corresponding to the average entanglement molecular weight, and g is the ratio of the square of the radius of gyration of the star to that of the linear molecule with the same molecular weight. Note that, for linear chains, the above representation is equivalent to the extensively used D/D_0 versus c/c^* scaling (D_0 is the extrapolated tracer diffusion at zero concentration c and c^* is the overlap concentration) when comparing solutions of the same polymer (constant N_e); for different N_e's, however, the N_e factor should also be taken into account.[32,22] In the present case of copolymers with the same composition, the N_e's are the same, and the N_e factor is irrelevant. Figure 11 shows the representation of the self-diffusion data for the three SB and TB pairs according to this scaling, where a collapse onto a master curve is evident when the total molecular weight is used. In the same plot, data are shown for the linear diblock copolymer SI-57 (MW = 159 000, $N = 1876$, $f_{PS} = 0.542$) from ref 22, which also fall on the same master plot.

Therefore, the differences in the self-diffusivities can be accounted for by the differences in the total molecular weight and the effect of the star architecture (g factor). The possibility of the interference of friction effects can be eliminated by utilizing the product of the self-diffusion coefficient, D_s, which is almost the same as the polydispersity diffusivity, D_p, times the longest relaxation time, τ_1, which is proportional to Γ_{int}^{-1} (eq 10b). It is predicted that $D_p\Gamma_{int}^{-1} \propto \phi^{-0.23}N$ for both Rouse and reptation regimes.[22,33] The inset of Figure 11 shows the concentration dependence of the product $D_p\Gamma_{int}^{-1}$, where agreement is observed with the $\phi^{-0.23}$ dependence. Since the Γ_{int}'s were shown to be the same between SB and TB (Figure 5 and eq 10), the observed difference in $D_p\Gamma_{int}^{-1}$ between the data for the two SB and TB pairs is due to the different total molecular weights of SB and TB affecting the diffusivities.

"Extra Process". It was shown above that at high concentrations the apparent intensities of the polydispersity process for SB-4 exhibit an extra dependence on the wavevector. This may be due to an extra "process" that is unresolved by the inverse Laplace transform analysis (eq 3). As discussed above, the extra intensity associate to this "phantom" process can be estimated as $\{I_p(q) - I_p(q\rightarrow 0)\}$ and increases with scattering angle, as evident from the data in Figure 8a; this extra intensity is shown in Figure 12 for the 90° scattering angle. The data exhibit a concentration dependence much stronger than ϕ^1, indicating an induced process. In a linear representation, this would mean that the intensities apparently do not go smoothly to zero at zero concentration, but it appears as if they are due to a process that develops above a certain concentration. One should also mention that although the presence of such extra intensity due to a mode that is unresolved by the analysis should in principle influence the dynamics, i.e., the q^2 dependence of the effective relaxation rate of the

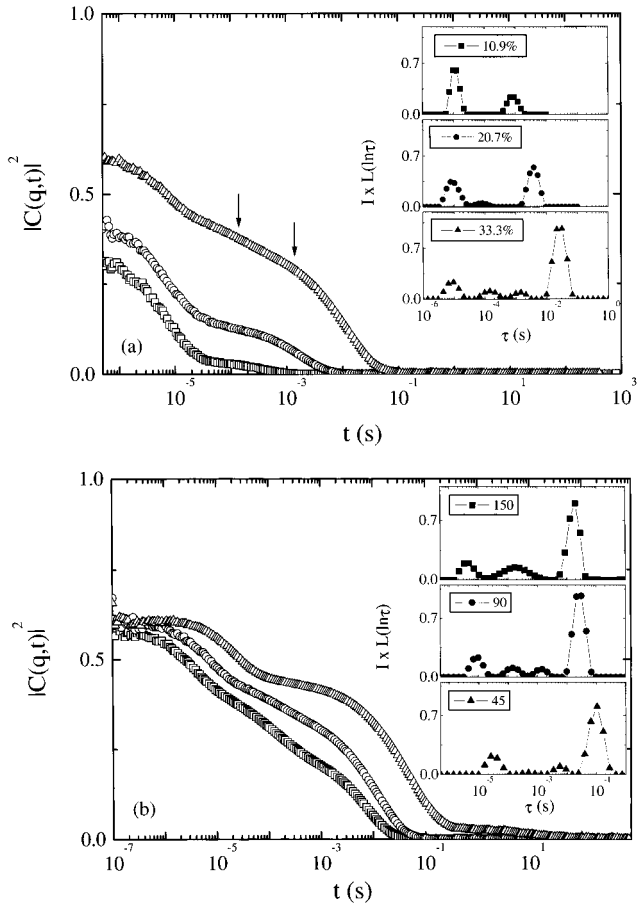

Figure 13. (a) Net polarized intensity correlation function at 90° scattering angle and 20 °C for 10.9 wt % (□, ■), 20.7 wt % (○, ●) and 33.3 wt % (△, ▲) disordered SB-2/toluene solutions. Insets: the corresponding distributions of the relaxation times $L(\ln \tau)$ multiplied by the total scattering intensity normalized to that of toluene I. The two arrows denote the two intermediate processes for 33.3 wt %. (b) Net polarized intensity correlation functions for a 33.3 wt % disordered SB-2/toluene solution at 20 °C for three different scattering angles 150° (□, ■), 90° (○, ●) and 45° (△, ▲). Insets: the corresponding distributions of the relaxation times $L(\ln \tau)$ multiplied by the total scattering intensity normalized to that of toluene I.

third mode in the correlation function, this is not really the case (Figure 8b), which suggests a contribution of a process with a q dependence in its rate.

To verify the existence of such a "process" which is hidden in the SB-4 system, the investigations for the SB-2 and SB-1 starblocks were extended to high concentrations still in the disordered state. Figure 13a shows the net polarized intensity autocorrelation functions at 90° scattering angle for the SB-2/toluene solutions for three different concentrations, with the distribution of relaxation times multiplied by the total polarized intensity normalized to that of toluene shown in the inset. The cooperative diffusion and the polydispersity mode are the only modes observed at 10.9 wt %, whereas the intermediate internal process is identified at 20.7 wt %. However, when the concentration is increased to 33.3 wt %, a fourth relaxation is observed between the internal and the polydispersity modes. The intensity of this process is of the same magnitude as that of the internal mode. Figure 13b shows the angular dependence of the net polarized intensity autocorrelation functions for the 33.3 wt % SB-2/toluene solution. Observation of the distribution of relaxation times in the insets shows the known behavior for the fast cooperative diffusion, the slow polydispersity mode, and the fast intermediate internal mode (see above) whereas the slow intermediate process shows an apparent q-independent amplitude together with a q-dependent rate. The low amplitude of the mode and its appearance as a separate process at angles less than 105° precludes the determination of the exact functional dependence of its rate (i.e., whether it is diffusive). However, its existence in the correlation functions is evident. Moreover, when a different solution of the inverse Laplace transform is chosen with only three processes, this leads to a loss of the known characteristics of the internal mode (in that case, the one intermediate process shows a q dependence of its rate) whereas the fit shows systematic deviations.

There are indications for the existence of such a process in the SB-1 system. However, in that case, this appears only above about 35 wt %; it has very low intensity, but, most importantly, it appears as a shoulder on the slow side of the internal mode (which is also observed at very high concentrations).

This extra process is observed near the ODT in the disordered state with the associated intensity I_{extra} exhibiting a strong concentration dependence (stronger than ϕ^1, as mentioned before) as shown in Figure 12 for all SB's; this corroborates the notion that the extra process is fluctuation-induced. Moreover, the dynamics of this process show a strong dependence on the molecular weight and on the block asymmetry parameter λ (these are the two differences among the SB samples): it is hidden close to the internal mode for the lowest molecular weight SB-1 ($\lambda = 0.5$) having $D_{extra}/D_p \cong 30$ (at ~40 wt %), and it is observed between the self-diffusion and the internal mode in SB-2 ($\lambda = 0.33$) with $D_{extra}/D_p \cong 15$ (at ~35 wt %), whereas it is apparently hidden together with the self-diffusion in the high molecular weight SB-4 ($\lambda = 0.2$), presumably having $D_{extra}/D_p \cong O(1)$.

The origin of such a process can only be speculated. We have shown earlier for high molecular weight entangled diblocks that two modes of structural relaxation[10] can be observed: one associated with the relaxation of composition fluctuations via a reptation mechanism and one related to the Rouse-like motion of the chains within their tubes; however in that case, the process that appears at higher concentrations (when the solution becomes entangled) is the faster of the two, and thus, it is by no means related to the possible process here. One may also envision such a mode to be related to a structural mode of an assembly of the starlike molecules due to a spatial correlation between star centers relaxing via collective rearrangement; such a mode has been recently observed[34] in solutions of multiarm stars homopolymers. That process was observed due to the finite contrast between the star-core region (more dense) and that away from the core, whereas its intensity was decreasing with concentration; in the present case of the four-arm SB the intensity increases with concentration faster that ϕ^1 (Figure 12).

An intermediate mode between the internal and the polydispersity processes has been also observed in only two cases of linear diblocks in the melt near the ODT;[35] it was actually designated as the "x-mode". In that case, the authors attributed the existence of such a diffusive process to the existence of remaining homopolymer in the diblock sample. However, PFG-NMR on the same

samples did not show a second diffusion process besides the normal self-diffusion of the diblock chains which corresponds to the polydispersity mode.[36] Moreover, a recent investigation of the dynamics of composition fluctuations in solutions of mixtures of a linear diblock with a homopolymer showed[37] that the addition of homopolymer of the same molecular weight mainly affects the characteristics (intensity and rate) of the so-called polydispersity mode without any indication of an extra, faster process.

A mode with characteristics similar to the one discussed herein has been recently observed in the correlation functions of solutions of A_2B simple graft copolymers, to be discussed in a subsequent paper.[38] Again in that case, the extra process appeared at high concentrations and actually above the concentration ϕ_e where entanglement effects should begin to become important and as the concentration of the three-arm star approaches the ODT. The preceding findings for SB's and A_2B's, along with the fact that there are no indications for the existence of such a process neither in the solutions of the linear tetrablocks nor in previous works on diblock copolymer solutions,[14−16,31] lead us to tentatively believe that this process is due to the starlike macromolecular architecture.

An unusual increase of the small-angle X-ray scattering intensity at the lowest accessible wavevectors (>0.14 nm^{-1}) was observed[39] in solutions of poly(styrene-*b*-isoprene-*b*-styrene), SIS, triblock copolymer in a neutral solvent (DOP) near the ODT in the disordered state. The increase of this intensity with temperature T above the T_{ODT} was ascribed to the enhanced osmotic compressibility between SIS and solvent, i.e., to total polymer concentration fluctuations. In our case, however, the intensity of the cooperative diffusion process, which is associated with this contribution, was found to depend on concentration similarly with that for semidilute homopolymer solutions.

On the theoretical side, the coexistence between disordered and ordered regions near the ODT for diblock copolymers in a good nonselective solvent is conceivable in the work of Fredrickson-Leibler.[13] The coexistence between solvent-rich disordered and solvent-poor ordered phases disappears at concentrations $\phi > \phi_{ODT}$. These spatial inhomogeneities may introduce an additional contribution to the osmotic compressibility, leading to scattering at low wavevectors. However, these dispersed particles of a new phase may also give rise to a scattering maximum at finite q even for a nucleation and growth mechanism;[40] i.e., the measured intensity at low q's may increase by increasing q. To address further the effect the proximity to the ODT, the 39.8 wt % SB-2/toluene solution, which was just ordered at 20 °C, was heated to 40 °C and measured. The correlation function at 40 °C (where the sample is disordered and apparently away from the ODT) did not show any indication of the existence of the extra process similarly to the situation at low concentrations. (The cooperative diffusion, the internal process, and the polydispersity mode were identified and behaved normally with the scattering wavevector.)

IV. Concluding Remarks

Photon correlation spectroscopy and pulsed-field-gradient NMR were used to investigate the effect of the macromolecular architecture on the relaxation of composition fluctuations in block copolymers at low wavevectors. Utilizing semidilute solutions of linear tetrablocks and inverse starblocks composed of two identical tetrablocks jointed at the middle, it has been shown that the concentration and composition fluctuations relax via the cooperative diffusion, the internal copolymer mode, and the polydispersity diffusive process, similarly to diblock copolymers. The relaxation of the composition fluctuations in the inverse starblock copolymer does not necessarily proceed with the longest relaxation time of the whole chain with the macromolecular architecture affecting the characteristic relaxation time. For the particular case of the tetrablock and the inverse starblock, the internal modes possess the same intensities and relaxation rates, meaning that linking together two tetrablocks into a single star does not change the polarization of each tetrablock chain. The self-diffusivities, on the other hand, show the effect of the molecular weight and the architecture. Evidence is also presented for the existence of an extra process for the starblock copolymers at high concentrations near the ODT between the polydispersity and the internal mode. The origin of such process is not understood at this time.

Acknowledgment. S.H.A., A.N.S., and N.H. acknowledge that part of this research was sponsored by NATO's Scientific Affairs Division in the framework of the Science for Stability Programme and by the Greek General Secretariat of Research and Technology. The financial support of the European Union in the framework of the Training and Mobility of Researchers Programme is acknowledged by G.F. and S.H.A. (contract FMRX-CT97-0112). G.Fl. acknowledges financial support from the Deutsche Forschungsgemeinschaft (SFB 294). We thank Ms. C. Lagiou for the light scattering measurements on SB-2, TB-2, and TB-1 and Mr. F. Rittig and Ms. A. Puhlmann for their help with the PFG-NMR measurements. We also thank Prof. T. Hashimoto for illuminating discussions and Dr. D. Vlassopoulos for his help regarding the rheological measurements.

References and Notes

(1) Bates, F. S.; Fredrickson, G. H. *Annu. Rev. Phys. Chem.* **1990**, *41*, 525. Bates, F. S. *Science* **1991**, *251*, 898. *Thermoplastic Elastomers−A Comprehensive Review*; Legge, R., Holden, N. R., Schroeder, H. E., Eds.; Hanser Publishers: Münich, 1988.

(2) Leibler, L. *Macromolecules* **1980**, *13*, 1602. Fredrickson, G. H.; Helfand, E. *J. Chem. Phys.* **1987**, *87*, 697. Barrat, G. L.; Fredrickson, G. H. *J. Chem. Phys.* **1991**, *95*, 1282.

(3) Fytas, G.; Anastasiadis, S. H. In *Disorder Effects on Relaxation Processes*; Richert, R., Blumen, A., Eds.; Springer-Verlag: Berlin, 1994; pp 697 and references therein.

(4) Stepanek, P.; Lodge, T. P. In *Light Scattering*; Brown, W., Ed.; Oxford University Press: Oxford, 1996 and references therein.

(5) Fredrickson, G. H.; Bates, F. S. *Annu. Rev. Phys. Chem.* **1996**, *26*, 501 and references therein.

(6) Fytas, G. *Macromol. Symp.* **1994**, *87*, 149. Fytas, G. *Macromol. Symp.* **1995**, *90*, 199. Fytas, G.; Chrissopoulou, K.; Anastasiadis, S. H.; Vlassopoulos, D.; Karatasos, K. In *Light Scattering and Photon Correlation Spectroscopy*; Pike, E. L., Abbiss, J. B., Eds.; NATO Advanced Science Institutes Series; Kluwer Academic Publishers: Dordrecht, The Netherlands, 1997; p 131.

(7) Anastasiadis, S. H.; Fytas, G.; Vogt, S.; Fischer, E. W. *Phys. Rev. Lett.* **1993**, *70*, 2415. Vogt, S.; Anastasiadis, S. H.; Fytas, G.; Fischer, E. W. *Macromolecules* **1994**, *27*, 4335. Fytas, G.; Anastasiadis, S. H.; Semenov, A. N. *Makromol. Chem., Macromol. Symp.* **1994**, *79*, 117. Semenov, A. N.; Fytas, G.; Anastasiadis, S. H. *Polym. Prepr.* **1994**, *35* (1), 618.

(8) Akcasu, A. Z.; Benmouna, M.; Benoit, H. *Polymer* **1986**, *27*, 1935. Benmouna, M.; Benoit, H.; Borsali, R.; Duval, M. *Macromolecules* **1987**, *20*, 2620. Akcasu, A. Z.; Tombakoglu,

M. *Macromolecules* **1990**, *23*, 607. Borsali, R.; Vilgis, T. A. *J. Chem. Phys.* **1990**, *93*, 3610. Borsali, R.; Fischer, E. W.; Benmouna, M. *Phys. Rev. A* **1991**, *43*, 5732.
(9) Erukhimovich, I. Ya.; Semenov, A. N. *Zh. Eksp. Teor. Fiz.* **1986**, *63*, 259 [*Sov. Phys. JETP* **1986**, *28*, 149].
(10) Semenov, A. N.; Anastasiadis, S. H.; Boudenne, N.; Fytas, G.; Xenidou, M.; Hadjichristidis, N. *Macromolecules* **1997**, *30*, 6280. Boudenne, N.; Anastasiadis, S. H.; Fytas, G.; Xenidou, M.; Hadjichristidis, N.; Semenov, A. N.; Fleischer, G. *Phys. Rev. Lett.* **1996**, *77*, 506.
(11) (a) Hashimoto, T.; Shibayama, M.; Kawai, H. *Macromolecules* **1983**, *16*, 1093. (b) Shibayama, M.; Hashimoto, T.; Hasegawa, H.; Kawai, H. *Macromolecules* **1983**, *16*, 1427. (c) Hashimoto, T.; Kowasaka, K.; Shibayama, M.; Kawai, H. *Macromolecules* **1986**, *19*, 754. (d) Hashimoto, T.; Mori, K. *Macromolecules* **1990**, *23*, 5347. (e) Lodge, T. P.; Pan, C.; Jin, X.; Liu, Z.; Zhao, J.; Maurer, W. W.; Bates, F. S. *J. Polym. Sci., Part B: Polym. Phys.* **1995**, *33*, 2289.
(12) Benmouna, M.; Benoit, H. *J. Polym. Sci., Part B: Polym. Phys.* **1983**, *21*, 1227. Benoit, H.; Wu, W.; Benmouna, M.; Mozer, B.; Bauer, B.; Lapp, A. *Macromolecules* **1985**, *18*, 986. Hong, K. M.; Noolandi, J. *Macromolecules* **1983**, *16*, 1083. Onuki, A.; Hashimoto, T. *Macromolecules* **1989**, *22*, 879. Olvera de la Cruz, M. *J. Chem. Phys.* **1989**, *90*, 1995.
(13) Joanny, J. F.; Leibler, L.; Ball, R. *J. Chem. Phys.* **1984**, *81*, 4640. Broseta, D.; Leibler, L.; Joanny, J. F. *Macromolecules* **1987**, *20*, 1935. Fredrickson, G. H.; Leibler, L. *Macromolecules* **1989**, *22*, 1238.
(14) Duval, M.; Haida, H.; Lingelser, J. P.; Gallot, Y. *Macromolecules* **1991**, *24*, 6867.
(15) Liu, Z.; Pan, C.; Lodge, T. P.; Stepanek, P. *Macromolecules* **1995**, *28*, 3221. Pan, C.; Mauer, W.; Liu, Z.; Lodge, T. P.; Stepanek, P.; von Meerwall, E. D.; Watanabe, H. *Macromolecules* **1995**, *28*, 1643.
(16) Jian, T.; Anastasiadis, S. H.; Semenov, A. N.; Fytas, G.; Adachi, K.; Kotaka, T. *Macromolecules* **1994**, *27*, 4762.
(17) Borsali, R.; Benoit, H.; Legrand, J.-F.; Duval, M.; Picot, C.; Benmouna, M.; Farago, B. *Macromolecules* **1989**, *22*, 4119. Duval, M.; Picot, C.; Benoit, H.; Borsali, R.; Benmouna, M.; Lartigue, C. *Macromolecules* **1991**, *24*, 3185.
(18) Olvera de la Cruz, M.; Sanchez, I. C. *Macromolecules* **1986**, *19*, 2501. Benoit, H.; Hadziioannou, G. *Macromolecules* **1988**, *21*, 1449. Mayes, A. M.; Olvera de la Cruz, M. *J. Chem. Phys.* **1989**, *91*, 7228. Mayes, A. M.; Olvera de la Cruz, M. *J. Chem. Phys.* **1991**, *95*, 4670. Dobrynin, A. V.; Erukhimovich, I. Ya. *J. Phys. II (Paris)* **1991**, *1*, 1387; *Macromolecules* **1993**, *26*, 276. Shinozaki, A.; Jasnow, G.; Balazs, A. C. *Macromolecules* **1994**, *27*, 2496.
(19) Koberstein, J. T.; Russell, T. P.; Walsh, D. J.; Pottick, L. *Macromolecules* **1990**, *23*, 877. Gehlsen, M. D.; Almdal, K.; Bates, F. S. *Macromolecules* **1992**, *25*, 939. Floudas, G.; Hadjichristidis, N.; Iatrou, H.; Pakula, T.; Fischer, E. W. *Macromolecules* **1994**, *27*, 7735. Floudas, G.; Hadjichristidis, N.; Tselikas, Y.; Erukhimovich, I. *Macromolecules* **1997**, *30*, 3090.
(20) Pochan, D. J.; Gido, S. P.; Pispas, S.; Mays, J. W.; Ryan, A. J.; Fairclough, J. P. A.; Hamley, I. W.; Terrill, N. J. *Macromolecules* **1996**, *29*, 5091. Pochan, D. J.; Gido, S. P.; Pispas, S.; Mays, J. W. *Macromolecules* **1996**, *29*, 5099.
(21) Tselikas, Y.; Hadjichristidis, N.; Lescanec, R. L.; Honeker, C. C.; Wohlgemuth, M.; Thomas, E. L. *Macromolecules* **1996**, *29*, 3390.
(22) Anastasiadis, S. H.; Chrissopoulou, K.; Fytas, G.; Fleischer, G.; Pispas, S.; Pitsikalis, M.; Mays, J.; Hadjichristidis, N. *Macromolecules* **1997**, *30*, 2445. Anastasiadis, S. H.; Chrissopoulou, K.; Fytas, G.; Appel, M.; Fleischer, G.; Adachi, K.; Gallot, Y. *Acta Polym.* **1996**, *47*, 250.
(23) Kärger, J.; Pfeifer, H.; Heink, W. *Adv. Magn. Reson.* **1988**, *12*, 1.
(24) Fleischer, G.; Fujara, F. NMR as a Generalized Scattering Experiment. In *NMR−Basic Principles and Progress*; Kosfeld, R., Blümich, B., Eds.; Springer-Verlag: Berlin, 1994; Vol. 30, p 159. Kärger, J.; Fleischer, G. *Trends Anal. Chem.* **1994**, *13*, 145.
(25) Jian, T.; Anastasiadis, S. H.; Fytas, G.; Adachi, K.; Kotaka, T. *Macromolecules* **1993**, *26*, 4706.
(26) It should be noted that $I(q)/N$ is proportional to the scattering intensity per copolymer chain, which is usually defined as the structure factor. However, in most theoretical works[2,18] the intensity $I(q)$ is calculated and is called structure factor.
(27) Benoit, H.; Anastasiadis, S. H., manuscript in preparation.
(28) Ham, J. S. *J. Chem. Phys.* **1957**, *26*, 625. Ferry, J. D. *Viscoelastic Properties of Polymers*; John Wiley: New York, 1980.
(29) Bueche, F. *J. Chem. Phys.* **1964**, *40*, 484. Berry, G. C.; Fox, T. G. *Adv. Polym. Sci.* **1968**, *5*, 261. Graessley, W. W.; Masuda, T.; Roovers, J. E. L.; Hadjichristidis, N. *Macromolecules* **1976**, *9*, 127. Roovers, J.; Graessley, W. W. *Macromolecules* **1981**, *14*, 766. Pearson, D. S.; Raju, V. R. *Macromolecules* **1982**, *15*, 294.
(30) de Gennes, P. G. *J. Phys. (Paris)* **1975**, *36*, 1199. Klein, J. *Macromolecules* **1986**, *19*, 105. McLeish, T. C. B.; Semenov, A. N. *Macromolecules* **1994**, *27*, 7205.
(31) Jian, T.; Anastasiadis, S. H.; Fytas, G.; Fleischer, G.; Vilesov, A. D. *Macromolecules* **1995**, *28*, 2439. Jian, T.; Fytas, G.; Anastasiadis, S. H.; Vilesov, A. D. *Polym. Mater. Sci. Eng.* **1994**, *71*, 767.
(32) Raspaud, E.; Lairez, D.; Adam, M. *Macromolecules* **1995**, *28*, 927.
(33) de Gennes, P. G. *Scaling Concepts in Polymer Physics*; Cornell University Press: Ithaca, NY, 1979. Doi, M.; Edwards, S. F. *The Theory of Polymer Dynamics*; Oxford Science Publishers: Oxford, 1986.
(34) Seghrouchni, R.; Petekidis, G.; Vlassopoulos, D.; Fytas, G.; Semenov, A. N.; Roovers, J.; Fleischer, G. *Europhys. Lett.* **1998**, *42*, 271.
(35) Stepanek, P.; Lodge, T. P. *Macromolecules* **1996**, *29*, 1244. Stepanek, P.; Almdal, K.; Lodge, T. P. *J. Polym. Sci., Part B: Polym. Phys.* **1997**, *35*, 1643.
(36) Fleischer, G.; Rittig, F.; Stepanek, P.; Almdal, K.; Papadakis, C. M. *Macromolecules* **1999**, *32*, 1956.
(37) Chrissopoulou, K.; Rittig, F.; Fytas, G. In *Molecular Interactions and Time-Space Organization in Macromolecular Systems*; Morishima, Y., Norisuye, T., Tashiro, K., Eds.; Springer-Verlag: Berlin, 1999.
(38) Chrissopoulou, K.; Harville, S.; Anastasiadis, S. H.; Fytas, G.; Mays, J. W.; Hadjichristidis, N. *J. Polym. Sci., Part B: Polym. Phys.*, in press.
(39) Sakamoto, N.; Hashimoto, T.; Han, C. D.; Kim, D.; Vaidya, N. Y. *Macromolecules* **1997**, *30*, 5321.
(40) Eliçabe, G. E.; Larrondo, H. A.; Williams, R. J. J. *Macromolecules* **1997**, *30*, 6550.

MA9901083